DFT Study on Mn-H Bond Dissociation Enthalpies of Manganese Hydrides in Manganese-Catalyzed Hydrogen Atom Transfer Reactions

Yan Que, Wenrui Zheng*, Chenhao Wu, Shenghao Pan and Peilei Jiao

College of Chemistry and Chemical Engineering, Shanghai University of Engineering Science

Shanghai 201620, China.

wrzheng@sues.edu.cn*

(Received on 14th June 2024, accepted in revised form 12th July 2025)

Summary: In recent years, metal-catalyzed hydrogen atom transfer (MHAT) reactions have become integral to many catalytic reactions due to their stereoselectivity, chemical fidelity and selectivity. As the first transition metal element in abundant global reserves, manganese has the advantages of lower price and less toxicity, and a series of manganese complexes are used in MHAT reactions. In the reaction, the prominent catalytic intermediate manganese hydride formation is involved in the whole catalytic cycle, therefore the rupture of manganese-hydrogen bonds denoted by one of the thermodynamic parameter of the Mn-H bond dissociation enthalpy (BDE) is essential. In the present research, the Mn-H BDEs of some manganese hydrides which have experimental values were computed by using several DFT functionals, and the data showed that the B3P86 functional provided the highest precision, which has the least root mean square error (RMSE) of 3.3 kcal/mol. In the following, the BDEs and substituent effects of ten kinds of manganese hydrides involved in manganese-catalyzed hydrogen atom transfer reactions were further explored, and the calculations showed that the ligand has a significant effect on Mn-H BDEs, and the effect of substituents on Mn-H BDEs varies in different types of manganese hydrides. Moreover, the natural bond orbital (NBO) as well as the energies of frontier orbitals analyses aimed at revealing the intrinsic factors of different patterns of change of the Mn-H BDE were accomplished.

Keywords: manganese hydrides; DFT; BDE; Manganese-catalyzed hydrogen atom transfer reactions; Mn-H bond

Introduction

The metal-catalyzed hydrogen atom transfer (MHAT) reactions have always been at the forefront of organic chemistry research because of its high atomic economy and simple operation, which meets the chemical requirements of green and sustainable development and has prominent industrial and academic significance in the generation of various molecular frameworks [1]. In recent decades, MHAT reactions became increasingly popular in several aspects, for example, Carreira [2-4], Shenvi [5-6], Herzon [7], Baran [8-9], Boger groups [10] and other experimental scientists extended the applications of MHAT reactions. The transition metal catalysts are of great interest due to their unusual reactivity and role as homogeneous catalysts in these MHAT reactions [11]. Early transition metals are attracting attention for their low cost, less toxicity and total sustainability [12-14], and in this respect, manganese, which is the third most abundant transition metal in the earth's crust, is used in these reactions replacing the precious late transition metal [15]. For example, as early as 1979, Tabushi *et al*. [16] utilized $NaBH_4$ and air to hydrate cyclohexene under Mn-catalyzed conditions. Rueping *et al*. [17] revealed that the hydrogenation and acceptor-free dehydrogenation of nitrogen-containing heterocycles can be fulfilled by the usage of a single manganese catalyst, in which manganese hydride plays an important role as a reaction intermediate. Milstein *et al*. [18] used manganese(I) complexes for the first time to catalyze cyclic imide hydrogenation to diols and amines. Milstein *et al*. [19] also reported that manganese complexes exhibited excellent catalytic activity in the hydrogenation of esters under mild conditions. Liu *et al*. [20] probed the Guerbet-type condensation reaction of ethanol to produce 1-butanol, resulting in upgrading ethanol into higher alcohols by using an efficient homogeneous manganese catalyst for the first time, and in the catalytic cycle proposals, the generation of Mn-H active intermediate is the key to the reaction. Since the report by Beller and colleagues in 2016 [21], manganese-catalyzed hydrogenation reactions have made tremendous progress. In the experimental catalytic systems, the manganese catalysts with tridentate PNP- and NNP-clamp ligands etc. were ubiquitous, which can hydrogenate aldehydes, aldehydes imides, ketones and

*To whom all correspondence should be addressed.

cyanide etc. [22-28]. For example, in 2018, Kirchner's research group [26] investigated homogeneous chemoselective hydrogenation of aldehydes in the condition of several hydride Mn(I) PNP pincer complexes, for example, the [Mn(PNP-*i*Pr)$(CO)_2$(H)] as catalysts. and the reaction can progress under base-free conditions with low catalyst loadings at room temperature. In 2019, Zhong's group [28] founded array of Mn(I) catalysts incorporating chiral imidazole-based PNN tridentate ligands, and the asymmetrical hydrogenation of benzophenones with excellent enantioselectivity can be achieved.

In summary, manganese hydride is a critical intermediate in manganese-catalyzed hydrogen atom transfer reactions, and the difficulties of the breaking of manganese-hydrogen bonds can illustrate the formation of manganese hydrides from a thermodynamic standpoint. Consequently, the bond dissociation enthalpy (BDE) of manganese-hydrogen bond in manganese hydrides, as one of the thermodynamic properties of Mn-H bond, is very indispensable for the comprehension of the overall catalytic cycle in manganese-catalyzed hydrogen atom transfer reactions. There are several universally available techniques for experimentally determining R-H bond energy in molecules, for example, photoionization mass spectrometry (PIMS), radical kinetic studies and acidic/electron affinity cycling. Unfortunately, reliable experimental data on bond dissociation energy are lacking in the entire field of organometallic chemistry, especially on metal-hydrogen bonding energy in coordinated saturated transition metal complexes of groups 6 to 12 [29]. However, with the swift advancement of density functional theory (DFT) in quantum chemistry, it is indisputable a robust and efficient computational tool for organic transition metal chemistry exploration, and the precise BDE computation of transition metal systems can be realized. For example, King *et al*. [30] explored a systematic contrast between DFTs and experimental results for the homoleptic mono- and multinuclear carbonyls for Mo, Tc, Ru, and Rh with X-ray crystallography determined structures. The 26 bond distances altogether have been calculated with each of DFTs and the average errors of BP86, B3LYP and MPW1PW91 are 0.030 Å, 0.028 Å and 0.018 Å, respectively. Weitz *et al*. [31] examined the relative energies of η^2-acyl-metal complexes including the η^1 and η^2-$CH_3C(O)Mn(CO)_4$ by the usage of DFT functionals. The data demonstrated that the BP86 and BLYP functionals gave the similar results and the calculated free energy differences between these complexes are consistent with the experimental data. Pandey *et al*. [32] utilized BP86, PBE and PW91 functionals to research the properties of the Mn≡E bond in the cationic *trans*-$[H(dmpe)_2Mn{\equiv}E(Mes)]^+$ (E=Ge, Sn) and $[H(dmpe)_2$-Mn≡Sn$(C_6H_3$-2,6-$Mes_2)]^+$ complexes, and the theoretical geometric parameters of the manganese-ylidyne complexes have a good consistency with the experimental values.

In the current research, different DFTs were assessed and the most appropriate one was selected to study the Mn-H BDE of manganese hydrides in manganese-catalyzed hydrogen atom transfer reactions. The geometries of the hydrides, the ligand effect of 14 different ligands, including PNP, NNP and NP ligands etc. [33-34], along with the substituent effects and the structure-activity relationships were systematically explored. It is favorable for the deeper comprehension of the hydrogen transfer process in Mn-catalyzed HAT reactions and it can also afford more theoretical directions for experimental researches.

Computational Methodology

The bond dissociation enthalpy (BDE) of the Mn-H bond in manganese hydrides is depicted as the enthalpy change of the following gas-phase reaction under the condition of 1 atm and 298.15 K.

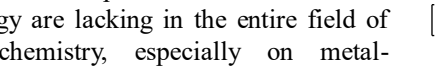

The enthalpy of each species is computed as:

$$H\,(298K) = E + H_{trans} + H_{rot} + H_{vib} + RT + ZPE$$

where H_{trans}, H_{rot} and H_{vib} are standard temperature correction items acquired from equilibrium statistical mechanics with rigid rotor and resonant oscillator approximations; the ZPE is the zero-point energy.

The B3LYP functional [35-36] and combined basis set with LANL2DZ for Mn and 6-31G(d) for other atoms were utilized in the optimization process of manganese hydrides and corresponding free radicals. Different geometries of each molecule and radical were compared and the frequency calculations were conducted at the same level to assure that each optimized conformation was an actual minimum. The eight DFT functionals including B3LYP [35-36], B3P86 [37], B97D [38], B97D3 [39], BP86 [40], BP86D3 [41], M05 [42] and M06 [43] were picked out

and assessed, which are used for the single-point energies computations with the combined basis set of SDD for Mn and 6-311++g (2df, 2p) for other atoms. The natural bond orbital (NBO) analysis was carried out by B3P86 functional with the combined basis set of SDD for Mn and 6-31+g(d) for other atoms. All calculations were implemented by means of Gaussian 16 package [44].

Results and Discussions

DFT assessment of Mn-H BDEs in manganese hydrides

In the beginning, we found five manganese hydrides which have the experimental Mn-H BDE values for the benchmarking, including the $Mn(CO)_5H$ and $Mn(CO)_5H^+$ with penta-coordinated carbonyl groups, in addition to $Mn(CO)_4(PEtPh_2)$-H and $Mn(CO)_4PPh_3$-H molecules coordinated by tetracarbonyls, along with ligand-free manganese hydrides [45-50]. Aimed at finding a relatively appropriate and precise functional to produce the BDEs of Mn-H bonds of different types of manganese hydrides, eight DFTs were picked out to calculate the BDEs of Mn-H of these five manganese hydrides, and the calculated results are shown in Table-1. Herein, the global-hybrid meta-GGA, for instance, M05 and M06 are contained, and there are also some dispersion corrections for functionals such as BP86D3, B97D and B97D3.

The correlation between the calculated data of the five Mn-H BDEs by 8 DFTs and the experimental values, expressed by the mean absolute deviation (MAD), the mean deviation (MD) and the root mean square error (RMSE) was demonstrated in Table-2. The data suggested that the B3P86 functional offers the best precision on Mn-H BDE, and the minimal RMSE is 3.3 kcal/mol, the MD and MAD are -0.6 and 2.9 kcal/mol, individually. Moreover, the RMSE, MD and MAD data of the B97D functional are 5.3, -3.6, and 4.1 kcal/mol individually, which has the second superior accuracy. Compared to B97D, the dispersion correction functional B97D3 does not afford better accuracy, which has a RMSE of 6.1 kcal/mol. Besides, the popular B3LYP functional has a comparatively lower precision in Mn-H BDE computation, and the MD, MAD, RMSE data are 0.2, 5.9 and 8.1 kcal/mol, individually.

As shown in Fig 1, a good linearity between B3P86 and experimental BDEs was discovered, with the correlation coefficient R^2 of 0.916. As can be seen from the above comparison, the B3P86 functional is the most suitable one to systematically explore the Mn-H BDEs along with substituent effects of different kinds of manganese hydrides in the following research.

In the experimental examples, manganese hydrides are indispensable active intermediates in the catalytic cycle. In addition, the spatial and electronic properties of the ligands can significantly affect the product properties and thus affect the event of the overall catalytic reaction, therefore, the designing and selection of appropriate ligands are of great significance for the optimization and development of metal catalysts with prominent catalytic activity and stereoselectivity [51]. Based on massive corresponding experimental researches, we sorted out ten manganese hydrides with different ligands, including PNP, NNP and NP ligands etc. (Mn-1~Mn-10), and their structures are shown in Fig 2.

Table-1: The Mn-H BDEs of five manganese hydrides calculated by 8 DFTs (kcal/mol).

Manganese hydrides	Exp. [45-50]	B3LYP	B3P86	B97D	B97D3	BP86	BP86D3	M05	M06
Mn-H	**38.9**	**54.0**	**35.5**	**30.0**	**30.8**	**20.4**	**21.7**	**24.0**	**54.0**
$Mn(CO)_5$-H	**65**	**61.6**	**65.4**	**62.7**	**61.4**	**64.5**	**65.2**	**60.4**	**61.6**
$Mn(CO)_4PPh_3$-H	**61**	**60.9**	**64.7**	**62.3**	**59.5**	**63.8**	**63.8**	**59.6**	**60.9**
$Mn(CO)_5$-H^+	**41.1**	**39.6**	**42.9**	**40.2**	**37.9**	**41.6**	**42.3**	**39.4**	**39.6**
$Mn(CO)_4(PEtPh_2)$-H	**71**	**61.9**	**65.8**	**63.7**	**61.3**	**65.1**	**65.2**	**61.1**	**61.9**

Table-2: The Correlation between calculated Mn-H BDEs by 8 DFTs and experimental data for five manganese hydrides (kcal/mol).

DFT	MD	MAD	RMSE	DFT	MD	MAD	RMSE
B3LYP	**0.2**	**5.9**	**8.1**	**BP86**	**-4.3**	**5.7**	**8.8**
B3P86	**-0.6**	**2.9**	**3.3**	**BP86D3**	**-3.8**	**5.4**	**8.2**
B97D	**-3.6**	**4.1**	**5.3**	**M05**	**-6.5**	**6.5**	**8.3**
B97D3	**-5.2**	**5.2**	**6.1**	**M06**	**0.2**	**5.9**	**8.1**

Note: MD (mean deviation) = $\Sigma(x_i-y_i)/N$; MAD (mean absolute deviation) = $\Sigma|x_i-y_i|/N$; RMSE (root mean square error) =$[\Sigma(x_i-y_i)^2/N]^{1/2}$ (N =5, x_i stands for the Mn-H BDEs of 8 DFTs, and y_i stands for the experimental Mn-H BDEs)

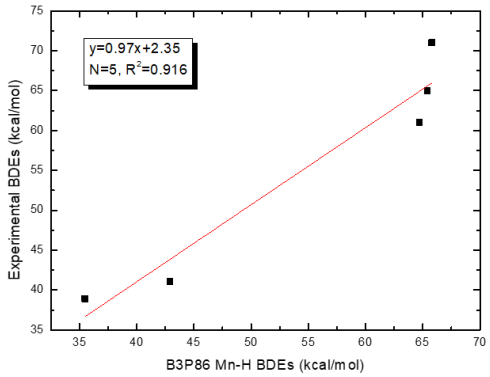

Fig. 1: The linearity between B3P86 and experimental Mn-H BDEs.

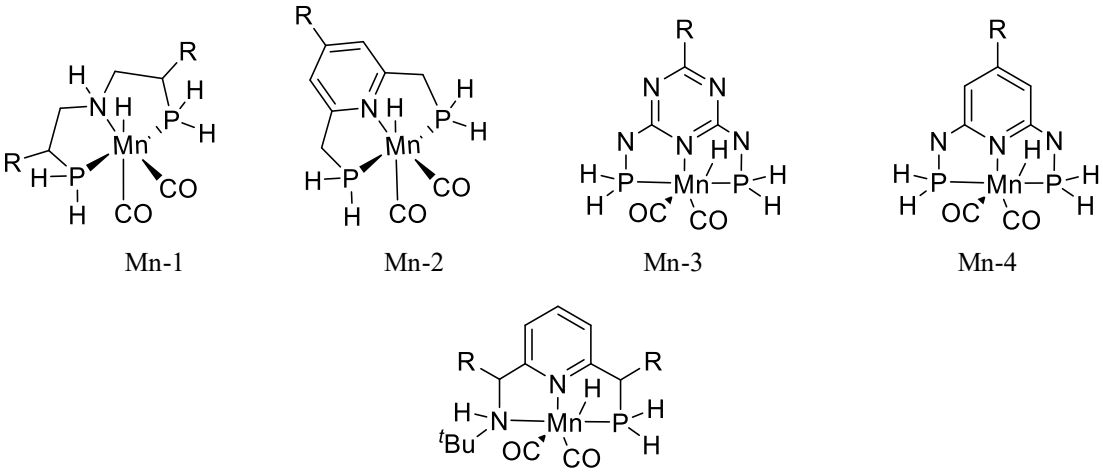

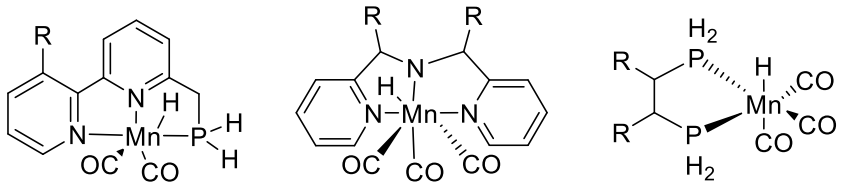

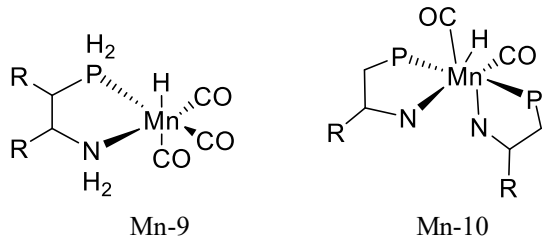

Fig. 2: The structures of typical manganese hydrides of Mn-1~Mn-10.

Geometries of manganese hydrides of Mn-1~Mn-10

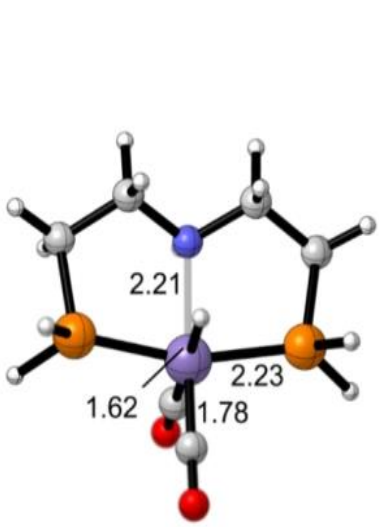

Mn-1

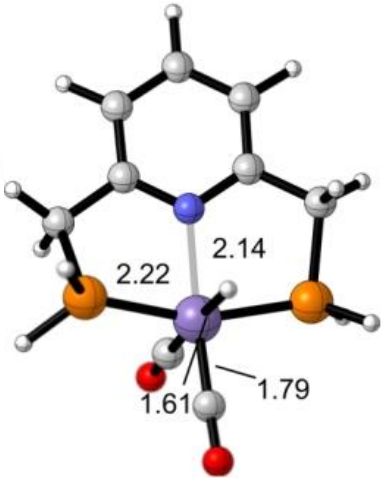

Mn-2

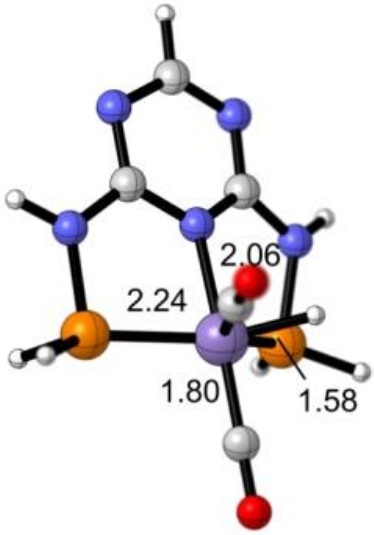

Mn-3

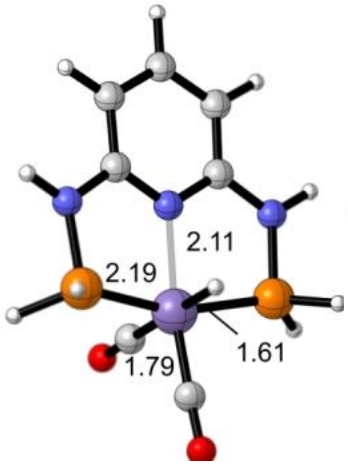

Mn-4

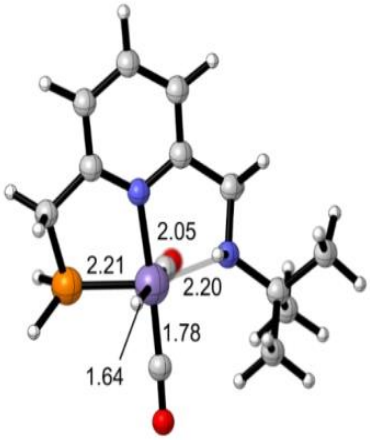

Mn-5

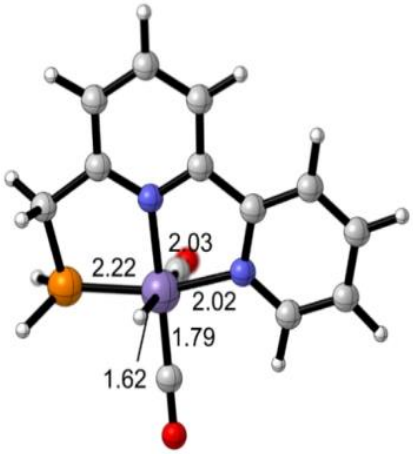

Mn-6

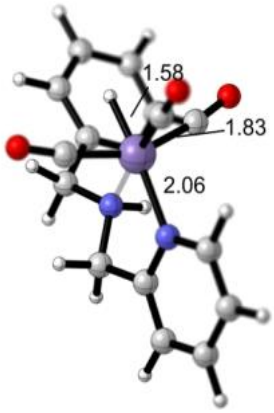

Mn-7

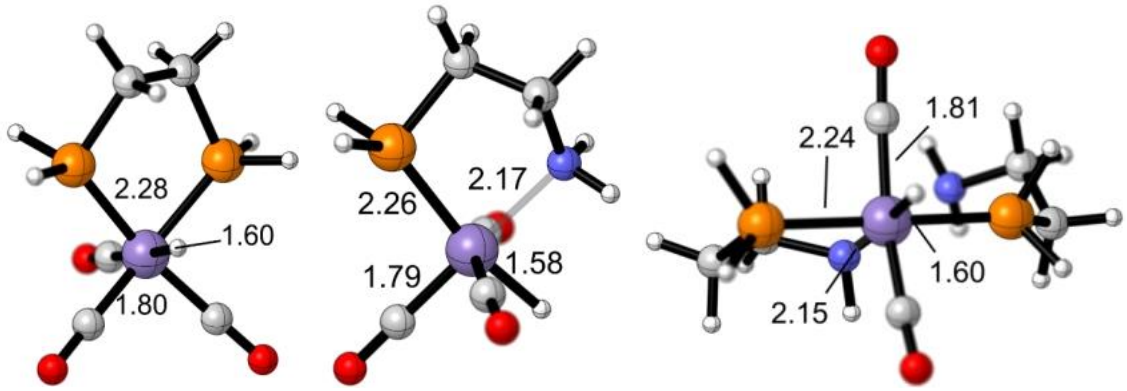

Mn- Mn-9 Mn-10

Fig. 3: The geometry diagram of Mn-1~Mn-10 (The bond length unit is Å).

For the ten manganese hydrides, the length range of Mn-H bond is 1.58 Å ~ 1.64 Å, and the Mn-H bond length of Mn-5 is the largest. The length ranges of Mn-N and Mn-P bonds are 2.03 Å ~ 2.21 Å and 2.19 Å ~ 2.28 Å, individually. The longest and shortest Mn-N bond lengths are found in Mn-1 and Mn-6, and the longest and shortest Mn-P bond lengths are found in Mn-4 and Mn-8 hydrides, separately. The length of Mn-C bond in these hydrides are 1.80 Å approximately. The Mn-1~Mn-10 presents different geometries due to the different coordination atoms and coordination manner of Mn atom.

Mn-H BDEs and substituent effect

Mn-H BDEs and substituent effect in ten manganese hydrides

The Mn-H BDEs of the above 10 manganese hydrides were computed by utilizing B3P86 functional, and the substituent effects of R (Fig.2) of -CF_3 (a typical electron-withdrawing group (EWG)) and -OH (a typical electron-donor group (EDG)) were explored. (Table-3).

For R=-H, the coverage of Mn-H BDEs is from 49.2 to 70.3 kcal/mol, with a large discrepancy of 21.1 kcal/mol. Herein, the hydride of Mn-9 has the largest BDE of 70.3 kcal/mol, followed closely by Mn-1 with 68.3 kcal/mol. The smallest Mn-H BDE data of 49.2 kcal/mol, was discovered in hydride of Mn-10. From the discrepancy of Mn-H data, it can be inferred that the ligands have a prominent effect on Mn-H BDEs in these manganese hydrides. By comparison with the results of the experimental researches, for the manganese hydrides Mn-1 and Mn-5, the Mn-H BDE of Mn-1 is larger than Mn-5, which indicated that Mn-1 is more stable than Mn-5 from the thermodynamic perspective. The experimental results showed that the reaction can be carried out under milder conditions catalyzed by the corresponding manganese catalyst of Mn-1 than Mn-5 [22]. To some extent, it shows that there is agreement between the theoretical calculations and the experimental results.

Table-3: The Mn-H BDEs with R=-OH and R=-CF_3 in ten hydrides (kcal/mol).

Manganese hydrides	Mn-H BDEs(R=-H)	Mn-H BDEs(R=-OH)	Mn-H BDEs(R=-CF_3)
Mn-1	**68.3**	**67.8**	**68.1**
Mn-2	**66.2**	**66.5**	**65.4**
Mn-3	**54.3**	**54.4**	**53.9**
Mn-4	**65.7**	**65.7**	**65.5**
Mn-5	**64.4**	**64.1**	**60.5**
Mn-6	**55.0**	**54.8**	**53.6**
Mn-7	**68.0**	**68.6**	**68.2**
Mn-8	**63.7**	**65.6**	**63.3**
Mn-9	**70.3**	**59.5**	**59.9**
Mn-10	**49.2**	**76.3**	**67.6**

We singled out two representative substituents, -OH and -CF_3, to initially investigate the substituent effects on Mn-H BDEs. In some manganese hydrides, the substituent effect is not pronounced. For instance, in Mn-1, the Mn-H BDE of R=-H is 68.3 kcal/mol, and the Mn-H BDEs of R=-OH and R=-CF_3 are 67.8 kcal/mol and 68.1 kcal/mol, individually. The identical effect of substituents on Mn-H BDEs was discovered in Mn-2, Mn-3, Mn-4, Mn-6, Mn-7 and Mn-8, and the disparity between R=-H, -OH and -CF_3 was found to be no more than 1.5 kcal/mol. For hydride Mn-5, the Mn-H BDE change is not significant when R equals -OH, while the Mn-H BDE goes down when R is -CF_3. In hydride of Mn-9, the Mn-H BDEs of R=-OH and R=-CF_3 greatly decline compared to R=-H, with a disparity of more than 10 kcal/mol. In addition, in Mn-10, there was a significant increase in Mn-H BDEs when the R is replaced by -OH and -CF_3.

To probe the substituent effects on Mn-H BDEs in Mn-5, Mn-9 and Mn-10 hydrides more deeply, the substituent effects of more substituents in these three manganese hydrides were thoroughly discussed.

Substituent effect in Mn-5, Mn-9 and Mn-10

Substituents extension was carried out by exploring the effect of more substituents in these three manganese hydrides on the Mn-H BDEs in Mn-5, Mn-9 and Mn-10 hydrides. The data of more substituents including different EWGs, EDGs and conjugation-effect groups (CEGs) are presented in Table-4.

The results demonstrated that the substituent effects on Mn-H BDEs in these three hydrides are differentiated. The Mn-H BDEs coverage of Mn-5 is between 60.5~64.6 kcal/mol, with a disparity of 4.1 kcal/mol. Both EDGs and EWGs diminish the BDEs of Mn-H comparing with R=-H. For instance, the hydride with R=-CF_3 has the minimal Mn-H BDE of 60.5 kcal/mol, and when R equals -OCH_3, the Mn-H BDE value is 64.1 kcal/mol. This suggests that EWGs have a greater impact than EDGs on Mn-H BDEs. For the CEG of R=-Ph, there is a tiny substituent effect on Mn-H BDE, and the Mn-H BDEs of R=-Ph and R=-H are 64.6 and 64.4 kcal/mol, individually.

In Mn-9 hydrides, the BDE value of Mn-H is significantly reduced compared to R=-H for all of the substituents. The BDE value range of Mn-H is 59.1~70.3 kcal/mol. When R=-$COOCH_3$, the BDE value of Mn-H decreased the most, with a difference of 11.2 kcal/mol, having a contrast to R=-H. The BDE values of the other substituents decreased by about 10 kcal/mol compared to R=-H.

In Mn-10 hydrides, the Mn-H BDEs coverage is between 45.3~76.9 kcal/mol, when R is replaced by EDGs, the BDE value of Mn-H significantly increased compared with R=-H. The EWGs can also increase Mn-H BDEs, except for R=-COOH and -$COOCH_3$, and the Mn-H BDEs of R=-COOH and -$COOCH_3$ are 48.0 and 45.3 kcal/mol, respectively.

NBO analysis of Mn-5, Mn-9 and Mn-10

NBO analytics of Mn-5

The single occupied molecular orbital (SOMO) energies of the corresponding radicals after the Mn-H breakage of Mn-5 with different substituents R are presented in Table-5. Except for R=-Ph, the E_{SOMO} of free radicals is less than the E_{SOMO} value of R=-H, and the BDEs of Mn-H are all less than the BDE value of R=-H. In addition, when R=-Ph, the E_{SOMO} of its free radicals is a little greater than that of E_{SOMO} when R equals -H, consistently, the BDE of Mn-H is also a little greater than the BDE value of R=-H. The higher E_{SOMO} indicates that free radicals are unstable and the larger Mn-H BDEs will be acquired.

Table-4: The substituent effect on Mn-H BDEs of Mn-5 and Mn-9 and Mn-10 hydrides (kcal/mol).

Entry	R	Mn-H BDEs		
		Mn-5	Mn-9	Mn-10
1	**-H**	**64.4**	**70.3**	**49.2**
2	**-OH**	**64.1**	**59.5**	**76.3**
3	**-OCH_3**	**64.1**	**59.5**	**68.6**
4	**-NH_2**	**62.0**	**59.3**	**76.9**
5	**-Ph**	**64.6**	**59.8**	**67.7**
6	**-CN**	**62.4**	**60.0**	**67.2**
7	**-COOH**	**63.9**	**59.4**	**48.0**
8	**-$COOCH_3$**	**63.9**	**59.1**	**45.3**
9	**-CF_3**	**60.5**	**59.9**	**67.6**

Table-5: The Mn-H BDEs (kcal/mol) and SOMO orbital energies of Mn-5 (Hartrees).

Entry	R	Mn-H BDEs	Radicals
			E_{SOMO}
1	-H	64.4	-0.1997
2	-OH	64.1	-0.2070
3	$-OCH_3$	64.1	-0.2027
4	$-NH_2$	62.0	-0.2010
5	-Ph	64.6	-0.1962
6	-CN	62.4	-0.2276
7	-COOH	63.9	-0.2065
8	$-COOCH_3$	63.9	-0.2019
9	$-CF_3$	60.5	-0.2153

The Fig 4 demonstrates the spin density data on Mn atom in corresponding free radicals of R=-H, $-NH_2$, -Ph, $-CF_3$, and the spin density on Mn is 0.6287 for R=-H. When R equals $-NH_2$ and R=$-CF_3$, the spin densities on the Mn are 0.6042 and 0.5683, individually, which are less than the spin density on the Mn of R=-H. The spin density value is 0.6986 for R=-Ph, which is greater than R=-H, and the BDE of Mn-H of R=-Ph is larger too. Therefore, the greater the spin density on the Mn in the center of the free radical, the more unstable the free radical, resulting in a higher BDE of Mn-H.

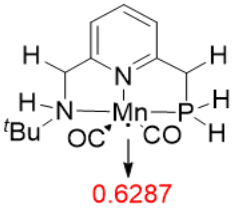

BDEs(kcal/mol) 64.4

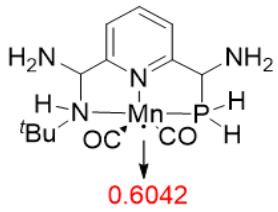

62.0

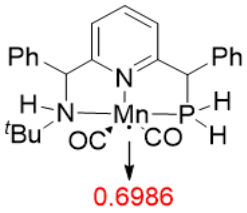

BDEs(kcal/mol) 64.6

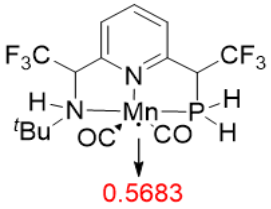

60.5

Fig. 4: The spin density data on Mn atom of R=-H, $-NH_2$, -Ph, $-CF_3$ in free radicals..

*NBO analytics of Mn-***9**

Table-6: The Mn-H BDEs (kcal/mol) along with the SOMO orbital energies of Mn-9 (Hartrees).

Entry	R	Mn-H BDEs	Radicals
			E_{SOMO}
1	-H	70.3	-0.1844
2	-OH	59.5	-0.1980
3	$-OCH_3$	59.5	-0.1959
4	$-NH_2$	59.3	-0.1916
5	-Ph	59.8	-0.1948
6	-CN	60.0	-0.2175
7	-COOH	59.4	-0.1994
8	$-COOCH_3$	59.1	-0.1955
9	$-CF_3$	59.9	-0.2093

Table-7: The Mn-H BDEs (kcal/mol) along with the natural charges on Mn in Mn-9 molecules and radicals.

Entry	R	Mn-H BDEs (kcal/mol)	Natural charges on Mn in molecules	Natural charges on Mn in radicals
1	-H	70.3	-0.8398	-0.4456
2	-OH	59.5	-0.8138	-0.4679
3	$-OCH_3$	59.5	-0.8133	-0.4691
4	$-NH_2$	59.3	-0.8155	-0.4637
5	-Ph	59.8	-0.8150	-0.4777
6	-CN	60.0	-0.8279	-0.4798
7	-COOH	59.4	-0.8193	-0.4655
8	$-COOCH_3$	59.1	-0.8188	-0.4633
9	$-CF_3$	59.9	-0.8223	-0.4773

The Table-6 shows the corresponding SOMO energies for Mn-9 after the Mn-H breakage. From the table, we can derive that the E_{SOMO} data are -0.1844 for R=-H, -0.1980 for R=-OH, and -0.2093 for R=-CF_3. The results show that when the R is replaced by EDGs, EWGs and CEGs, the E_{SOMO} of free radicals decreases, and then the BDE value of Mn-H also diminishes, which reveals that the lower E_{SOMO} is, the more stable the free radicals are, and the smaller Mn-H BDEs will be obtained.

Moreover, the Table-7 lists the natural charges on Mn in the Mn-9 molecules along with the natural charges on Mn in the equivalent radicals. It reveals that the natural charges on Mn in the molecules are mainly centralized in the coverage of -0.8398~-0.8133. When the R is displaced by EDGs, EWGs and CEG, the natural charges on Mn in the molecule are larger than those on Mn in the molecules of R=-H. For instance, when R equals -OH, the natural charge on Mn is -0.8398, when R equals -CF_3, the natural charge on Mn is -0.8223, simultaneously, the BDE value of Mn-H for R =-CF_3 is less than the BDE of R =-H. The distribution of natural charges in the molecules suggests that induction and conjugation effects exhibited by EDGs and EWGs are crucial to Mn-H BDE and its variation patterns.

Meanwhile, the variation pattern of natural charges on Mn in the equivalent substituted radicals can also interpretate the BDEs of Mn-H. The conclusion can be drawn from the table, it is, different substituents can raise the natural charges on Mn in molecules and weaken the natural charges on Mn in free radicals. For instance, when R equals -H, the natural charge data on Mn in free radicals is -0.4456, and when R equals -OH and -CF_3, the natural charge data on Mn in radicals are -0.4679 and -0.4773, individually. Simultaneously, except for R =-H, there exists a good linearity between the natural charge data on Mn in the free radicals with the BDEs of Mn-H, as shown in Fig 5, with R^2 of 0.944 and the slope of 0.95.

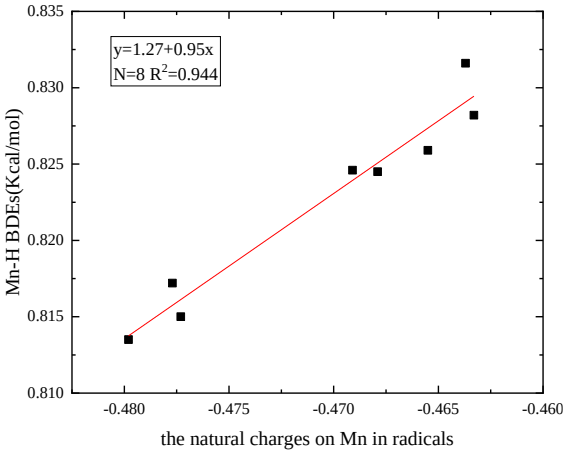

Fig.5: The linearity between natural charge data on Mn in Mn-9 radicals and Mn-H BDEs.

NBO analytics of Mn-10

Table-8: The Mn-H BDEs (kcal/mol) along with the natural charges on Mn atoms in Mn-10 molecules with different R.

Entry	R	Mn-H BDEs	Natural charges on Mn in molecules
1	-H	49.2	-0.3428
2	-OH	76.3	-0.5806
3	$-OCH_3$	68.6	-0.5678
4	NH_2	76.9	-0.5773
5	-Ph	67.7	-0.5696
6	-CN	67.2	-0.5755
7	-COOH	48.0	-0.2770
8	$-COOCH_3$	45.3	-0.2770
9	$-CF_3$	67.6	-0.5689

The Table-8 presents the natural charge data on Mn in the Mn-10 molecules with different R, which can interpretate the variation pattern of BDE of Mn-H. When R equals -H, the natural charges on Mn is -0.3248, when R equals -COOH and -$COOCH_3$, the natural charge data on Mn atoms are both -0.2770, and

when the R is displaced by other substituents, the natural charges on Mn are in the coverage of -0.5806~-0.5687. Likewise, the Mn-H BDEs of Mn-H of R=-COOH and -$COOCH_3$ are less than that of R=-H, and the Mn-H BDE data for the rest of the substituents are greater than R=-H. The smaller the natural charge data on Mn in molecules, the Mn-H BDEs are larger.

Notably, for R=-COOH, -$COOCH_3$, the Mn-H BDEs are smaller comparing with other EWGs, and the Fig 6 lists the spin density data on Mn in free radicals of R=-H, -OH, -CF_3, -COOH, and -$COOCH_3$. For R=-H, the spin density data on Mn atom is -0.0090, while for R=-OH and -CF_3, the spin density on Mn atoms are more centralized on Mn, and the data are 0.2201 and 1.5128, individually. For R=-COOH and -$COOCH_3$, the spin density data on Mn diminish to -0.0134 and -0.0152, respectively, and a powerful delocalization effect was discovered, consequently, their free radicals are more stable, leading to a decrease in the corresponding Mn-H BDEs.

Comprehensive comparison of Mn-5, Mn-9 and Mn-10

There exhibited different substitution effects in these three manganese hydrides of Mn-5, Mn-9 and Mn-10. In Mn-5, the EDGs and EWGs diminish the Mn-H BDEs, and the CEG (-Ph) increases Mn-H BDEs. In Mn-9, all substituent of EWGs, EDGs, or CEGs significantly reduce Mn-H BDEs. In Mn-10, except for R=-COOH and -$COOCH_3$, the remaining substituents will significantly increase Mn-H BDEs. The variation pattern of BDEs can be interpreted by the energy analysis of the single-occupancy molecular orbital of free radicals (E_{SOMO}). The Mn-H BDEs data increases with the increase of E_{SOMO}. For instance, in Mn-5, when R equals -H, the E_{SOMO} of the free radical is -0.1997 Hartrees and its BDE is 64.4 kcal/mol. For R=-OH and R=-COOH, the E_{SOMO} data of free radicals are -0.2070 and -0.2065 Hartrees, and the corresponding BDEs are 64.1 kcal/mol and 63.9 kcal/mol, individually. In Mn-9, the E_{SOMO} of free radicals is -0.1844 Hartrees for R=-H, and its BDE is 70.3 kcal/mol, and for R=-OH and R=-COOH, its values are -0.1980 and -0.1994 Hartrees, and the corresponding BDEs are 59.5 and 59.4 kcal/mol, individually. In Mn-10, when R equals -H, -OH and R=-COOH, the E_{SOMO} of free radicals are -0.2394, -0.2153 and -0.2443 Hartrees, individually, while the corresponding Mn-H BDE data are 49.2 kcal/mol, 76.3 kcal/mol and 48.0 kcal/mol, individually. The Fig 7 demonstrates the SOMO diagrams of typical substituents of -OH and -COOH in Mn-5, Mn-9, and Mn-10 radicals, which visually reflect the differences in charge delocalization in their free radicals.

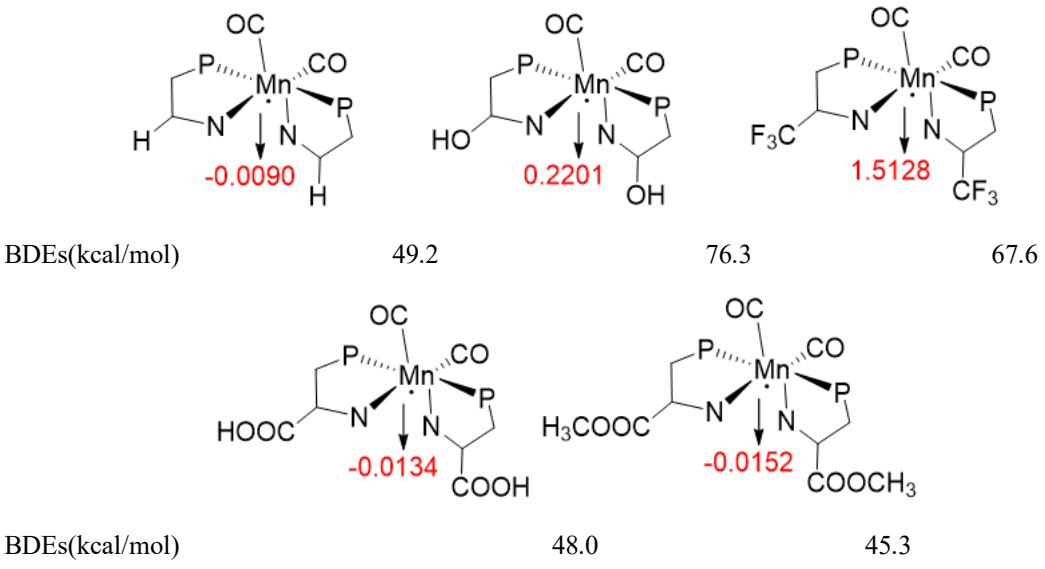

Fig. 6: The Spin density data on Mn in free radicals of R=-H, -OH, -CF_3, -COOH and -$COOCH_3$.

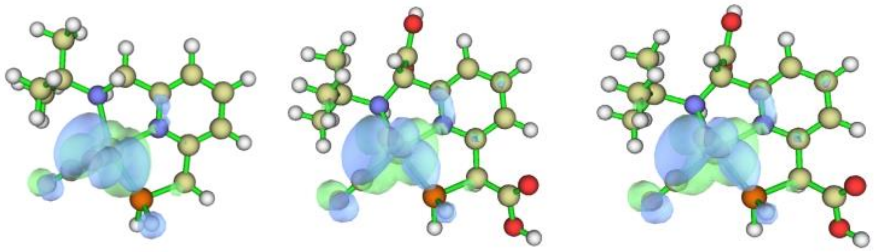

Mn-5 E_{SOMO} (Hartrees)	-0.1997	-0.2070	-0.2065
Mn-5 BDEs (kcal/mol)	64.4	64.1	63.9
	A	B	C

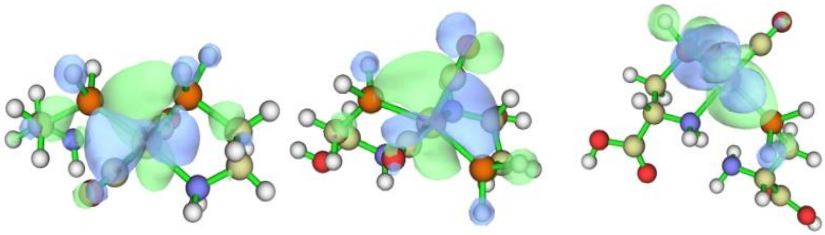

Mn-9 E_{SOMO} (Hartrees)	-0.1844	-0.1980	-0.1994
Mn-9 BDEs (kcal/mol)	70.3	59.5	59.4
	A	B	C

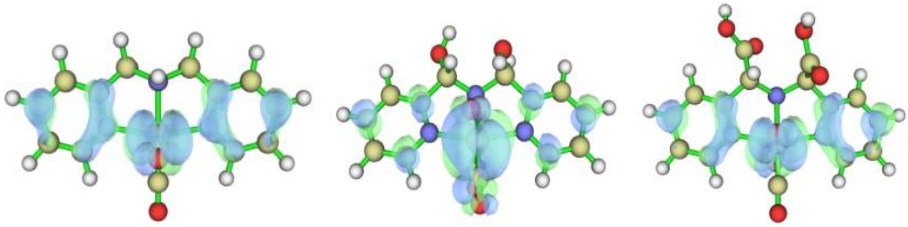

Mn-10 E_{SOMO} (Hartrees)	-0.2394	-0.2153	-0.2443
Mn-10 BDEs (kcal/mol)	49.2	76.3	48.0
	A	B	C

Fig. 7: The SOMO diagrams of Mn-5, Mn-9 and Mn-10 radicals of R=-H(corresponding to A), -OH(corresponding to B) and -COOH(corresponding to C).

Comprehensive comparison of Mn-5 and Mn-6

In the Mn-5 hydride, the substituent has a pronounced effect on Mn-H BDE, while in Mn-6, the substitution has a small effect and its frame structure is similar to that of Mn-5. In Mn-5, the natural charge data on Mn atoms in its molecule changes significantly after being displaced by different substitutes of R. For R=-H, and $-CF_3$, the natural charge data on Mn are -0.5346 and -0.5569, individually. In contrast, the natural charge data on Mn in the Mn-6 molecule differs by merely about 0.002 *e* after being displaced by $-CF_3$ (Fig 8). Moreover, the variation of the natural charges on H atom in the Mn-5 molecule is noteworthy after being displaced by different substitutes, while the variation in Mn-6 hydride is insignificant.

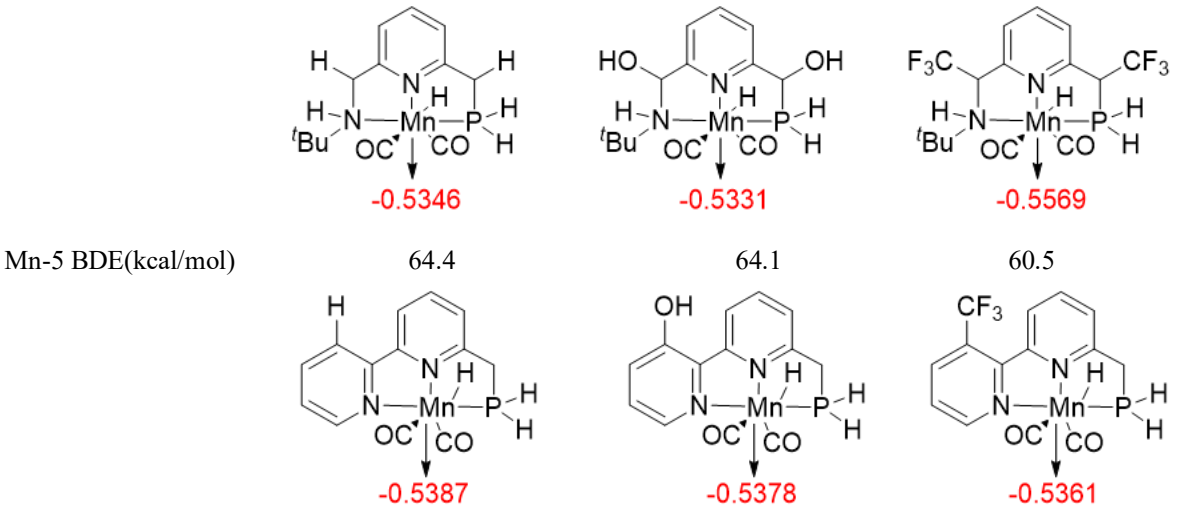

Fig. 8: The natural charge data on Mn atoms in Mn-5 and Mn-6 molecules.

Conclusion

In the current research, we sorted out five manganese hydrides which have experimental Mn-H BDE data as our training set in benchmarking step and performed Mn-H BDEs computation with eight DFT functionals. The calculational results indicated that the B3P86 functional is optimal with the least RMSE of 3.3 kcal/mol. As a result, the Mn-H BDEs of ten kinds of manganese hydrides with different ligands in manganese-catalyzed hydrogen atom transfer reactions along with the substituent effects were systematically explored by utilizing B3P86 functional. The major findings are:

First, the substituent effects on Mn-H BDEs of two representative substituents (-OH and -CF_3) in 10 manganese hydrides were probed, which indicated that in Mn-1, Mn-2, Mn-3, Mn-4, Mn-6, Mn-7 and Mn-8 hydrides, the substituents on Mn-H BDEs is not distinguishing. However, the substituent effect on Mn-H BDEs in Mn-5, Mn-9, and Mn-10 hydrides is prominent.

The further substituent effects for more substituents were investigated and the results indicated that in Mn-5, both EDGs and EWGs can diminish the Mn-H BDEs, and EWGs have a greater influence than EDGs. In addition, the CEG increases Mn-H BDE. Except for R=-Ph, the E_{SOMO} of free radicals of different substituents is smaller than that of R=-H, and Mn-H BDEs are all smaller than that of R=-H. While for R=-Ph, the E_{SOMO} of the free radical is greater than that of R=-H, and Mn-H BDE is also greater than that of R=-H. Furthermore, the spin density data on Mn in the free radicals displaced by EDGs and EWGs is less than those on Mn when R equals -H, while for R=-Ph, the spin density is larger than that on Mn for R=-H. Hence, the larger the spin density on Mn in the center of the free radical, the more unstable the free radical is, resulting in a higher Mn-H BDE.

In Mn-9, both EDGs and EWGs can significantly diminish Mn-H BDEs. The results showed that when the R is displaced by EDGs, EWGs and CEG, the free radical E_{SOMO} decreases, and Mn-H BDE also decreases. In addition, after the R is displaced by EDGs, EWGs and CEG, the natural charge data on Mn in the molecules are all larger than those on Mn in the molecule when R equals -H, meanwhile, Mn-H BDEs are all smaller than that of Mn-H BDE of R=-H. Besides R=-H, there is a good linearity between the natural charge data on Mn in the free radicals with the Mn-H BDEs.

In Mn-10, except for R=-COOH and -$COOCH_3$, both EDGs and EWGs can significantly increase Mn-H BDEs. When R=-COOH and -$COOCH_3$, Mn-H BDEs are less than Mn-H BDE of R=-H. For R=-COOH and -$COOCH_3$, the natural charges on Mn in the molecules are smaller than that when R=-H, in addition, for R=-COOH and -$COOCH_3$,

the spin density data on Mn decreases greatly, and the strong delocalization results in the decrease of corresponding Mn-H BDE value. From these two aspects, it can be explained that when R=-COOH and -$COOCH_3$, Mn-H BDE is less than Mn-H BDE of R=-H.

Overall, we can see that the Mn-5, Mn-9 and Mn-10 manganese hydrides have different substituent effects, and Mn-H BDEs increase with the increase of the free radical E_{SOMO} of these three molecules, which may explain the change pattern of Mn-H BDEs. In these 10 manganese hydrides, different Mn-H BDEs change patterns are shown. For structurally similar frames, such as Mn-5 and Mn-6, the natural charge data on Mn in the molecules vary prominently after being displaced by different substituents of R in Mn-5, which is not the case in Mn-6 hydride.

Acknowledgment

This project is funded by the Shanghai University of Engineering Science Innovation Fund for Undergraduate Students (No. cs2404003). We also thank the Shanghai Supercomputer Center for the computational resources.

References

1. S. W. M. Crossley, C. Obradors, R. M. Martinez and R. A. Shenvi, Mn-, Fe-, and Co-Catalyzed Radical Hydrofunctionalizations of Olefins, *Chem. Rev.*, **116**, 8912 (2016).
2. J. Waser and E. M. Carreira, Convenient synthesis of Alkylhydrazides by the Cobalt-catalyzed Hydrohydrazination Reaction of Olefins and Azodicarboxylates, *J. Am. Chem. Soc.*, **126**, 5676 (2004).
3. J. Waser and E. M. Carreira, Catalytic Hydrohydrazination of a Wide Range of Alkenes with a Simple Mn Complex, *Angew. Chem. Int. Ed.*, **43**, 4099 (2004).
4. J. Waser, H. Nambu and E. M. Carreira, Cobalt-Catalyzed Hydroazidation of Olefins: Convenient Access to Alkyl Azides, *J. Am. Chem. Soc.*, **127**, 8294 (2005).
5. S. W. M. Crossley, F. Barabé and R. A. Shenvi, Simple, Chemoselective, Catalytic Olefin Isomerization, *J. Am. Chem. Soc.*, **136**, 16788 (2014).
6. K. Iwasaki, K. K Wan, A. Oppedisano, S. W. M. Crossley and R. A. Shenvi, Simple, Chemoselective Hydrogenation with Thermodynamic Stereocontrol, *J. Am. Chem. Soc.*, **136**, 1300 (2014).
7. S. M. King, X. Ma and S. B. Herzon, A Method for the Selective Hydrogenation of Alkenyl Halides to Alkyl Halides, *J. Am. Chem. Soc.*, **136**, 6884 (2014).
8. M. Yan, J. C. Lo, J. T. Edwards and P. S. Baran, Radicals: Reactive Intermediates with Translational Potential, *J. Am. Chem. Soc.*, **138**, 12692 (2016).
9. J. C. Lo, Y. Yabe and P. S. Baran, A Practical and Catalytic Reductive Olefin Coupling, *J. Am. Chem. Soc.*, **136**, 1304 (2014).
10. J. E. Sears and D. L. Boger, Total Synthesis of Vinblastine, Related Natural Products, and Key Analogues and Development of Inspired Methodology Suitable for the Systematic Study of Their Structure–Function Properties, *Acc. Chem. Res.*, **48**, 653 (2015).
11. E. S. Wiedner, M. B. Chambers, C. L. Pitman, R. M. Bullock, A. J. M. Miller and A. M. Appel, Thermodynamic Hydricity of Transition Metal Hydrides, *Chem. Rev.*, **116**, 8655 (2016).
12. W. Ai, R. Zhong, X. Liu and Q. Liu, Hydride Transfer Reactions Catalyzed by Cobalt Complexes, *Chem. Rev.*, **119**, 2876 (2019).
13. I. Bauer and H.-J. Knölker, Iron Catalysis in Organic Synthesis, *Chem. Rev.*, **115**, 3170 (2015).
14. N. Gorgas and K. Kirchner, Isoelectronic Manganese and Iron Hydrogenation/Dehydrogenation Catalysts: Similarities and Divergences, *Acc. Chem. Res.*, **51**, 1558 (2018).
15. K. Das, M. K. Barman and B. Maji, Advancements in Multifunctional Manganese Complexes for Catalytic Hydrogen Transfer Reactions, *Chem. Commun.*, **57**, 8534 (2021).
16. I. Tabushi and N. Koga, P-450 Type Oxygen Activation by Porphyrin-manganese Complex, *J. Am. Chem. Soc.*, **101**, 6456 (1979).
17. V. Zubar, J. C. Borghs and M. Rueping, Hydrogenation or Dehydrogenation of N-Containing Heterocycles Catalyzed by a Single Manganese Complex, *Org. Lett.*, **22**, 3974 (2020).
18. U. K. Das, T. Janes, A. Kumar and D. Milstein, Manganese Catalyzed Selective Hydrogenation of Cyclic Imides to Diols and Amines, *Green Chem.*, **22**, 3079 (2020).
19. N. A. Espinosa-Jalapa, A. Nerush, L. J. W. Shimon, G. Leitus, L. Avram, Y. Ben-David and D. Milstein, Manganese-Catalyzed Hydrogenation of Esters to Alcohols, *Chem. Eur. J.*, **23**, 5934 (2017).

20. S. Fu, Z. Shao, Y. Wang and Q. Liu, Manganese-Catalyzed Upgrading of Ethanol into 1-Butanol, *J. Am. Chem. Soc.*, **139**, 11941 (2017).
21. S. Elangovan, C. Topf, S. Fischer, H. Jiao, A. Spannenberg, W. Baumann, R. Ludwig, K. Junge and M. Beller, Selective Catalytic Hydrogenations of Nitriles, Ketones, and Aldehydes by Well-Defined Manganese Pincer Complexes, *J. Am. Chem. Soc.*, **138**, 8809 (2016).
22. A. Mukherjee and D. Milstein, Homogeneous Catalysis by Cobalt and Manganese Pincer Complexes, *ACS Catal.*, **8**, 11435 (2018).
23. F. Kallmeier, T. Irrgang, T. Dietel and R. Kempe, Highly Active and Selective Manganese C=O Bond Hydrogenation Catalysts: The Importance of the Multidentate Ligand, the Ancillary Ligands, and the Oxidation State, *Angew. Chem. Int. Ed.*, **55**, 11806 (2016).
24. S. Elangovan, M. Garbe, H. Jiao, A. Spannenberg, K. Junge and M. Beller, Hydrogenation of Esters to Alcohols Catalyzed by Defined Manganese Pincer Complexes, *Angew. Chem. Int. Ed.*, **55**, 15364 (2016).
25. R. van Putten, E. A. Uslamin, M. Garbe, C. Liu, A. Gonzalez-de-Castro, M. Lutz, K. Junge, E. J. M. Hensen, M. Beller, L. Lefort and E. A. Pidko, Non-Pincer-Type Manganese Complexes as Efficient Catalysts for the Hydrogenation of Esters, *Angew. Chem. Int. Ed.*, **56**, 7531 (2017).
26. M. Glatz, B. Stöger, D. Himmelbauer, L. F. Veiros and K. Kirchner, Chemoselective Hydrogenation of Aldehydes under Mild, Base-Free Conditions: Manganese Outperforms Rhenium, *ACS Catal.*, **8**, 4009 (2018).
27. V. Zubar, Y. Lebedev, L. M. Azofra, L. Cavallo, O. El-Sepelgy and M. Rueping, Hydrogenation of CO_2-Derived Carbonates and Polycarbonates to Methanol and Diols by Metal-Ligand Cooperative Manganese Catalysis, *Angew. Chem. Int. Ed.*, **57**, 13439 (2018).
28. F. Ling, H. Hou, J. Chen, S. Nian, X. Yi, Z. Wang, D. Song and W. Zhong, Highly Enantioselective Synthesis of Chiral Benzhydrols via Manganese Catalyzed Asymmetric Hydrogenation of Unsymmetrical Benzophenones Using an Imidazole-Based Chiral PNN Tridentate Ligand, *Org. Lett.*, **21**, 3937 (2019).
29. J. A. M. Simões and J. L. Beauchamp, Transition Metal-Hydrogen and Metal-Carbon Bond Strengths: The Keys to Catalysis, *Chem. Rev.*, **90**, 629 (1990).
30. X. Feng, J. Gu, Y. Xie, R. B. King and H. F. Schaefer III, Homoleptic Carbonyls of the Second-Row Transition Metals: Evaluation of Hartree-Fock and Density Functional Theory Methods, *J. Chem. Theory Comput.*, **3**, 1580 (2007).
31. X. Wang and E. Weitz, A Density Functional Theory Study of η^2 Acyl Bonding in Fe and Mn Carbonyl Complexes, *J. Phys. Chem. A*, **106**, 11782 (2002).
32. K. K. Pandey, P. Patidar and R. Vishwakarma, Relevance of Dispersion Interactions in the Germylidyne and Stannylidyne Complexes of Manganese: Structure and Bonding-Energy Analysis, *Eur. J. Inorg. Chem.*, **2014**, 2916 (2014).
33. G. A. Filonenko, R. van Putten, E. J. M. Hensen and E. A. Pidko, Catalytic (de)hydrogenation Promoted by Non-Precious Metals-Co, Fe and Mn: Recent Advances in An Emerging Field, *Chem. Soc. Rev.*, **47**, 1459 (2018).
34. Y. Wang, L. Zhu, Z. Shao, G. Li, Y. Lan and Q. Liu, Unmasking the Ligand Effect in Manganese-Catalyzed Hydrogenation: Mechanistic Insight and Catalytic Application, *J. Am. Chem. Soc.*, **141**, 17337 (2019).
35. A. D. Becke, Density-Functional Exchange-Energy Approximation with Correct Asymptotic Behavior, *Phys. Rev. A*, **38**, 3098 (1988).
36. C. Lee, W. Yang and R. G. Parr, Development of the Colle-Salvetti Correlation-Energy Formula into a Functional of the Electron Density, *Phys. Rev. B*, **37**, 785 (1988).
37. J. P. Perdew, Density-Functional Approximation for the Correlation Energy of the Inhomogeneous Electron Gas, *Phys. Rev. B*, **33**, 8822 (1986).
38. S. Grimme, Semiempirical GGA-Type Density Functional Constructed with a Long-Range Dispersion Correction, *J. Comput. Chem.*, **27**, 1787 (2006).
39. A. Austin, G. A. Petersson, M. J. Frisch, F. J. Dobek, G. Scalmani and K. Throssell, A Density Functional with Spherical Atom Dispersion Terms, *J. Chem. Theory Comput.*, **8**, 4989 (2012).
40. H. Hirao, Which DFT Functional Performs Well in the Calculation of Methylcobalamin? Comparison of the B3LYP and BP86 Functionals and Evaluation of the Impact of Empirical Dispersion Correction, *J. Phys. Chem. A*, **115**, 9308 (2011).
41. J. Yang and M. P. Waller, A Systematic Approach to Identify Cooperatively Bound Homotrimers, *J. Phys. Chem. A*, **117**, 174 (2013).
42. Y. Zhao, N. E. Schultz and D. G. Truhlar, Exchange-Correlation Functional with Broad Accuracy for Metallic and Nonmetallic Compounds, Kinetics, and Noncovalent Interactions, *J. Chem. Phys.*, **123**, 161103 (2005).

43. Y. Zhao and D. G. Truhlar, Density Functionals with Broad Applicability in Chemistry, *Acc. Chem. Res.*, **41**, 157 (2008).
44. M. J. Frisch, G. W. Trucks, H. B. Schlegel, G. E. Scuseria, M. A. Robb, J. R. Cheeseman, G. Scalmani, V. Barone, G. A. Petersson, H. Nakatsuji, X. Li, M. Caricato, A. V. Marenich, J. Bloino, B. G. Janesko, R. Gomperts, B. Mennucci, H. P. Hratchian, J. V. Ortiz, A. F. Izmaylov, J. L. Sonnenberg, D. Williams-Young, F. Ding, F. Lipparini, F. Egidi, J. Goings, B. Peng, A. Petrone, T. Henderson, D. Ranasinghe, V. G. Zakrzewski, J. Gao, N. Rega, G. Zheng, W. Liang, M. Hada, M. Ehara, K. Toyota, R. Fukuda, J. Hasegawa, M. Ishida, T. Nakajima, Y. Honda, O. Kitao, H. Nakai, T. Vreven, K. Throssell, J. A. Montgomery, Jr., J. E. Peralta, F. Ogliaro, M. J. Bearpark, J. J. Heyd, E. N. Brothers, K. N. Kudin, V. N. Staroverov, T. A. Keith, R. Kobayashi, J. Normand, K. Raghavachari, A. P. Rendell, J. C. Burant, S. S. Iyengar, J. Tomasi, M. Cossi, J. M. Millam, M. Klene, C. Adamo, R. Cammi, J. W. Ochterski, R. L. Martin, K. Morokuma, O. Farkas, J. B. Foresman and D. J. Fox, Gaussian, Inc., *Gaussian 16, Revision C.01*, Wallingford CT (2019).
45. M. Tilset and V. D. Parker, Solution Homolytic Bond Dissociation Energies of Organotransition-Metal Hydrides, *J. Am. Chem. Soc.*, **111**, 6711 (1989).
46. R. G. Pearson, The Transition-Metal-Hydrogen Bond, *Chem. Rev.*, **85**, 41 (1985).
47. D. D. M. Wayner and V. D. Parker, Bond Energies in Solution from Electrode Potentials and Thermochemical Cycles. A Simplified and General Approach, *Acc. Chem. Res.*, **26**, 287(1993).
48. P. B. Armentrout and B. L. Kickel, Gas-Phase Thermochemistry of Transition Metal Ligand Systems: Reassessment of Values and Periodic Trends, *Organometallic Ion Chemistry*, **15**, 1 (1996).
49. T. Ziegler, V. Tschinke and A. Becke, Theoretical Study on the Relative Strengths of the Metal-Hydrogen and Metal-Methyl Bonds in Complexes of Middle to Late Transition Metals, *J. Am. Chem. Soc.*, **109**, 1351 (1987).
50. J. Uddin, C. M. Morales, J. H. Maynard and C. R. Landis, Computational Studies of Metal-Ligand Bond Enthalpies across the Transition Metal Series, *Organometallics*, **25**, 5566 (2006).
51. S. L. Buchwald and D. Milstein, *Ligand Design in Metal Chemistry: Reactivity and Catalysis*, John Wiley & Sons (2016).